Journal of Dynamics, Monitoring and Diagnostics, 2025, 4, 121-136
https://doi.org/10.37965/jdmd.2025.806

ISTP
RESEARCH ARTICLE

Development of a Digital Model of a Gear Rotor System for Fault Diagnosis Using the Finite Element Method and Machine Learning

Anubhav Srivastava and Rajiv Tiwari
Department of Mechanical Engineering, Indian Institute of Technology Guwahati, Guwahati, India

(Received 01 May 2025; Revised 12 May 2025; Accepted 04 June 2025; Published online 04 June 2025)

Abstract: Geared-rotor systems are critical components in mechanical applications, and their performance can be severely affected by faults, such as profile errors, wear, pitting, spalling, flaking, and cracks. Profile errors in gear teeth are inevitable in manufacturing and subsequently accumulate during operations. This work aims to predict the status of gear profile deviations based on gear dynamics response using the digital model of an experimental rig setup. The digital model comprises detailed CAD models and has been validated against the expected physical behavior using commercial finite element analysis software. The different profile deviations are then modeled using gear charts, and the dynamic response is captured through simulations. The various features are then obtained by signal processing, and various ML models are then evaluated to predict the fault/no-fault condition for the gear. The best performance is achieved by an artificial neural network with a prediction accuracy of 97.5%, which concludes a strong influence on the dynamics of the gear rotor system due to profile deviations.

Keywords: digital model; finite element modeling; gear profile errors; geared-rotor system; machine learning

I. INTRODUCTION

Gear constitutes one of the most vital components used in mechanical systems. They are extensively used for transmitting motion and power from simple to very complex mechanical systems. With the continuously growing demands of gear systems, specifically in very high-speed applications, it is essential to achieve precise gearing action. The *fundamental law of gearing* is essential to ensure the smooth and continuous transmission of motion between gears. Despite the best manufacturing technologies and best practices followed across the industry, it is impossible to obtain ideal involute tooth profiles, which are essential to abide as per law of gearing. Apart from that, the elastic deformation of gears during meshing and gear tooth wear adds to further errors and deviations of gear tooth profiles. The gear profile deviations have an adverse effect on gear transmission errors (TE). It is defined as the difference between the actual position of the driven gear and the ideal position the gear would have occupied if the driving and driven gears were of perfect conjugate profile. It sets gear mesh in continuous contact without any deformation of gear mesh [1].

Ghosh and Chakraborty [1] mentioned noise, vibrations, and reduced efficiency in mechanical systems as source of transmission errors which mainly arise due to profile deviations, assembly errors, elastic deformations, and wear and lubrication issues. TE arises due to various types of faults associated with gears. The gear faults can be broadly classified as operational faults, which are caused during gear operation and tooth profile faults, which may be present due to initial manufacturing errors or may occur due to operational faults, like wear. Mohammed and Rantatalo [2] classified the gear operational faults into two major classes based on (i) lubrication-related failures: overload failure and bending fatigue failure, which are independent of the system's lubrication and bound to occur with time; and wear, pitting, and scuffing, which depend on the lubrication of the system that is lubrication directly impacts these failure by smoothening the interaction between gear tooth and (ii) location-related failures: wear, pitting, scuffing and flank overload, which occur on the tooth flank, whereas root overload and bending fatigue failure occur at the tooth fillets near the root. The various types of operational defects arising in gears are as follows: (i) *Cracks and breakage* occur by initiation of cracks at gear root, (ii) *Gear tooth wear* caused by wearing of gear tooth by subsequent operations, (iii) *Pitting and spalling* resulting in formation of large pits due to surface fatigue failure, (iv) *Scuffing or scoring* (*adhesive wear*), which is the surface failure occurring due to lack of lubrication. Figure 1 depicts various classes of tooth profiles and deviations in gears. The L_α corresponds to the length over which profile deviations are evaluated. The profile deviations include the following: (i) *Total Profile Deviation* (F_α): It refers to the distance between the actual profile trace, (ii) *Profile Slope Deviation* ($f_{H\alpha}$) [3]: It refers to the distance between the design profile line and the mean profile line, measured at the tip diameter, (iii) *Profile Form Deviation* ($f_{f\alpha}$): It refers to the distance between the two facsimiles of the mean profile trace, to enclose the actual mean profile trace, and (iv) *Profile Crown* (C_α) refers to modification given to the tooth surface with a small amount of curvature.

Various researchers have tried exploiting tooth profile modifications and errors to attain a smoother gear dynamic. On one hand, gear tooth profile errors are inevitable, whereas tooth modifications are intentionally made to compensate for the degradation in performance due to profile errors. Tesfahunegn *et al.* [4] studied tooth profile modifications at the tip to compensate for deflections under load, modeling them in linear and parabolic forms and

Corresponding authors: Anubhav Srivastava and Rajiv Tiwari (e-mails: anubhav.3410@iitg.ac.in and rtiwari@iitg.ac.in).

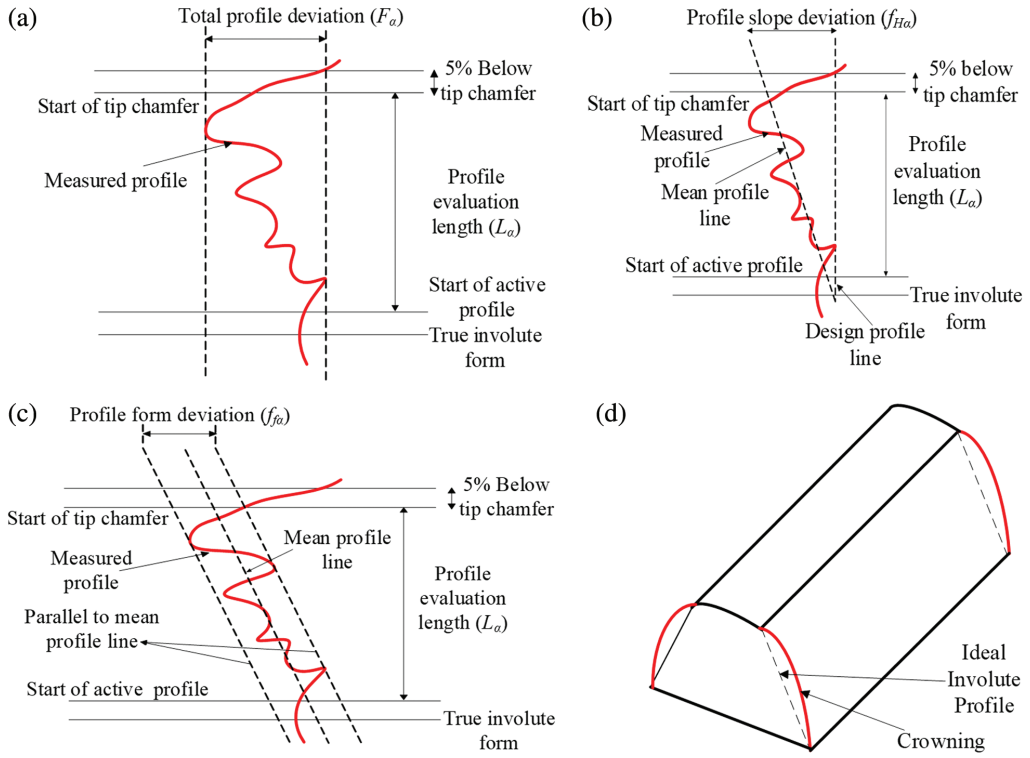

Fig. 1. Gear tooth profile deviations: (a) Total profile deviation, (b) Profile slope deviation, (c) Profile form deviation, and (d) Profile crown.

establishing the strong effect of modification on gear strength. Ma *et al.* [5] discussed the tooth profile modifications belonging to three classes, tip relief, root relief, and whole tooth profile modification, and presented the equation for modeling profile modification curve at the tip. Bonori and Pellicano [6] analyzed the non-linear vibration of spur gears in the presence of manufacturing errors treating them stochastically and modeled composite profile error represented by first four harmonics of the Fourier Series as in equation (1)

$$e_{PE} = \sum_{k=1}^{4} E_k \cos(k\widetilde{\omega}_m t - \gamma_k) \text{ with } \widetilde{\omega}_m = \frac{\omega_m}{N_g N_p} \quad (1)$$

where E_k and γ_k are amplitudes and phases, N_g and N_p are the number of teeth on gear and pinion, respectively, and ω_m is the gear mesh frequency. Mucchi *et al.* [7] considered the profile deviations in the study of the dynamics of the gear pump and modeled them as a summation constant term depicting slope deviation and a sinusoidal term depicting form deviation. Fernández *et al.* [8] analyzed gear dynamics incorporating tooth profile deviations and modeled as sinusoidal shapes with amplitude $f_{f\alpha}$ and f_r cycles as

$$e_{PE}(s) = f_{H\alpha}\frac{(s-s_0)}{(s_f-s_0)} + \frac{f_{f\alpha}}{2}\sin\left\{2\pi f_r \frac{(s-s_0)}{(s_f-s_0)}\right\} \quad (2)$$

where $f_{f\alpha}$ is the profile form deviation, $f_{H\alpha}$ is the profile slope deviation, s is the roll path length, measured along tangent to base circle, and s_0 and s_f correspond to the starting and end point on the involute. Zheng *et al.* [9] established a model considering tooth profile deviations and modeling the tooth profile error as a series of cosine functions as

$$e_{PE} = \sum_{n=1}^{N} A_{ern} \cos\left(\frac{2\pi n\beta}{\theta_{g0}} + \varphi_{ern}\right) \quad (3)$$

where A_{ern} and φ_{ern} represent the amplitude and phase of the nth cosine, respectively, and θ_{g0} and β represent the angle at which the gear teeth turn from entering to exiting the meshing area and represent the position corresponding point on the tooth profile. The vibration-based condition monitoring and integration of machine learning in the same has been a trending topic of research. Mohammed and Rantatalo [2] discussed the significance of condition-based monitoring (CBM) in reducing failures and unplanned stoppages in gear systems. Sharma and Parey [10] discussed the various signal parameters that have been used for various fault predictions in gear systems. Researchers have tried deriving various analytical and finite element models to study the gear mesh dynamics, which is the main parameter to implement CBM in gear systems. Chen *et al.* [11] analyzed time-varying mesh stiffness and transmission errors as key excitations in gear meshing through an analytical model validated against FEM results. Chen and Ji [12] developed an analytical model to study the effects of tooth profile modifications, wear, corner contact, and structural coupling on gear mesh stiffness.

Zheng *et al.* [9] improved existing analytical models of gear mesh by directly incorporating tooth profile deviations, extended contact, and structural coupling along with profile deviation. Saxena *et al.* [13] performed a modal analysis of a gear rotor system using ANSYS Workbench, obtaining mode shapes and corresponding frequencies. Tiwari [14] discussed the detailed analysis of torsional and transverse vibration of rotor systems using one-dimensional FEM elements. Visnadi *et al.* [15] developed finite element model of a gear rotor system to study gear mesh stiffness

variations due to cracks. Liu *et al.* [16] discussed the integration of a digital twin (DT), which is a virtual representation of a physical object, process, or system coupled via real-time data for CBM. Kritzinger *et al.* [17] classified the concept of digital twin based on level of data integration between physical and virtual entities: (i) Digital model which does not use any form of automated data exchange and (ii) Digital shadow with one-way data flow and (iii) Digital twin with fully integrated flow of data.

Further, the integration of machine learning to automate CBM for fault diagnosis is being widely used. Praveenkumar *et al.* [18] used a support vector machine model to detect faulty and non-faulty gears based on wear criterion by acquiring vibration signals. Gecgel *et al.* [19] studied the performance of machine learning and deep learning models for fault classification in gear tooth profiles using analytically simulated data. Lupea and Lupea [20] implemented multi-class classification and studied the performance of various classifier algorithms to analyze mounting faults in an experimental rotor system setup. Das *et al.* [21] discussed the various works done, for fault identification in various elements of the rotor system using machine learning (ML). The literature review has been done to start with the transmission error and fault introduction in gears and then narrowed down to the profile deviation. Subsequently, the profile modeling and work performed on the CBM, digital twin, and finally application of the ML.

Through this work, the aim is to develop the digital model of single-stage gearing, giving more flexibility to introduce different profile deviations and modeling them in a realistic manner and develop a machine learning model to predict the deviations based on the dynamic response obtained from the system. For the same, the existing experimental rig setup is used as a reference and step-by-step development, and validation of components is done. Figure 2 depicts the flowchart giving an insight into the step-by-step process followed for the study. The gear profiles are derived from a gear chart to exactly replicate them in the digital model, which is conventionally lacking in current work and has been achieved by fitting the harmonic series. The work also becomes crucial with respect to the industrial aspect, where the coordinate measuring probe-based gear testers are used to benchmark the obtained gear profiles against the required standards. This becomes a time-consuming task in industries for quality testing, only considering three/four gear teeth for measuring deviations.

II. SYSTEM MODELING

There are various assumptions which have been considered for subsequent development of the model and are mentioned as (i) the developed components have been considered as linear, isotropic, and homogenous, (ii) loads applied are well within the elastic range of the components (iii) defects except profile deviation have not been considered in the CAD models, (iv) thermal considerations along with wear and tear during the operational aspect are ignored, and (v) a few components in the model have been replaced with their equivalent boundary conditions. Figure 3 depicts the experimental setup from which the numerical model is derived. Motor of 1 HP was used to power the system, which drives the input shaft connected via flexible coupling

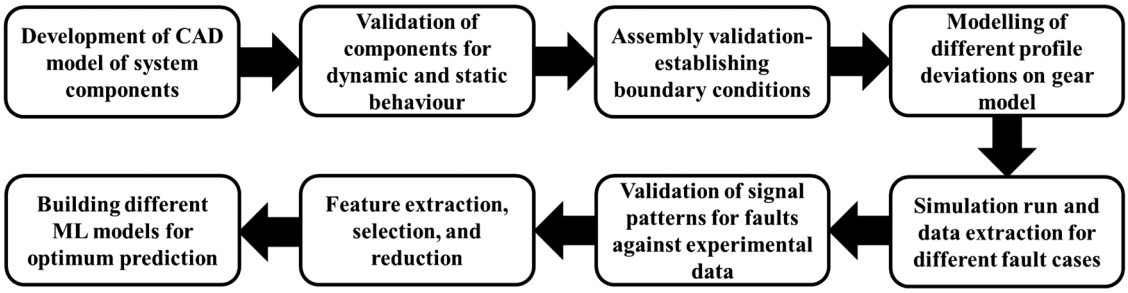

Fig. 2. Flowchart concluding the procedure followed to develop the digital model.

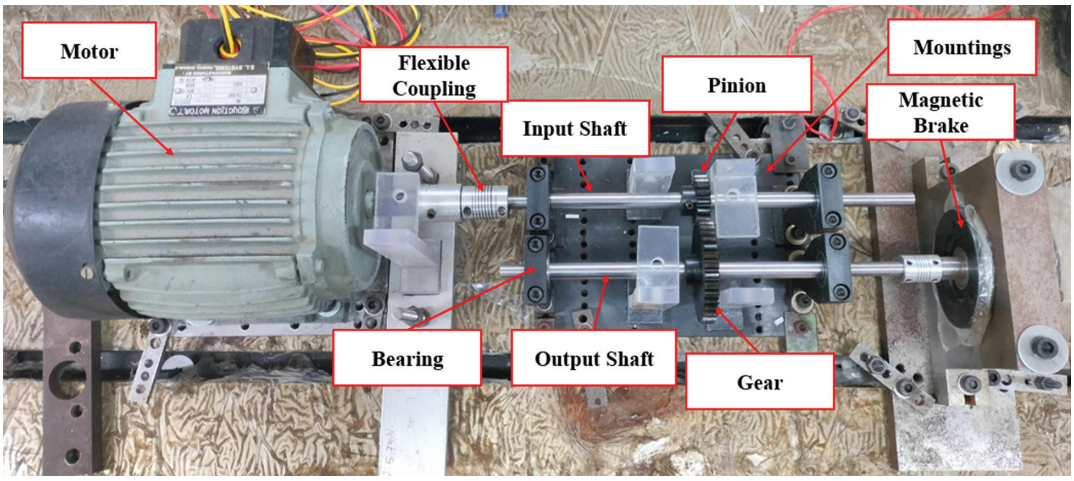

Fig. 3. Experimental rig setup.

Table I. Specification of the shaft

Sr. No.	Parameter	Particulars
	Material properties	
1	Material name	Steel
2	Density	7850 kg/m^3
3	Young's modulus, E	2.1×10^{11} Pa
4	Poisson's ratio, v	0.3
	Physical measurements	
5	Number of steps	2
6	Number of segments	3
7	Total length	295 mm
8	Segment-wise length	Segment 1: 70 mm
		Segment 2: 190 mm
		Segment 3: 35 mm
9	Segment-wise diameter	Segment 1: 10 mm
		Segment 2: 12 mm
		Segment 3: 10 mm

Table II. Pinion and gear parameters used in the experimental rig

Sr. No.	Parameter	Pinion	Gear
	Geometric properties		
1	Type of profile	Involute	Involute
2	Number of teeth	16	35
3	Module (mm)	2	2
4	Pressure angle (°)	20	20
5	Pitch circle diameter (mm)	32	70
6	Base circle diameter (mm)	30.07	65.778
7	Addendum (mm)	2	2
8	Dedendum (mm)	2.5	2.5
9	Total height of tooth (mm)	4.5	4.5
10	Addendum diameter (mm)	36	74
11	Dedendum diameter (mm)	27	65
12	Profile/addendum shift coefficient (x_{mc})	0	0
13	Root fillet radius (mm)	1.381	1.415
14	Clearance (mm)	0.5	0.5
15	Tooth thickness (mm)	3.1416	3.14229
16	Space width (mm)	3.1416	3.14229
17	Backlash (mm)	0	0
18	Bore diameter (mm)	12	12
	Material properties		
	Young's Modulus (E)	210 GPa	210 GPa
	Poisson's ratio (v)	0.3	0.3

to the motor. The pinion is mounted on the input shaft, which further meshes with the output shaft. Deep groove ball bearings support both the input and output shaft at each of the ends. A magnetic brake is used in the model, which prevents free rotation of the gear and ensures continuous mesh between the pinion and the gear. The mountings are used to fix the model over the cast iron bed. The equivalent digital model mainly consists of the modeling of the following components: shafts, pinion, and gears and replacing the rest of the components by equivalent boundary conditions. Tables I–III depict the attributes of each of the components. Figure 4 depicts the rendered CAD model images of the components.

Table III. Highlights the bearing dimensions used in the experimental rig

Sr. No.	Parameter	Value (mm)
1	Inner race groove radius of curvature (r_i)	4.86
2	Outer race groove radius of curvature (r_o)	4.95
3	Ball diameter (D_b)	4.76
4	Bore diameter (d)	10
5	Outer diameter (D)	26
6	Bearing pitch diameter (D_m)	18

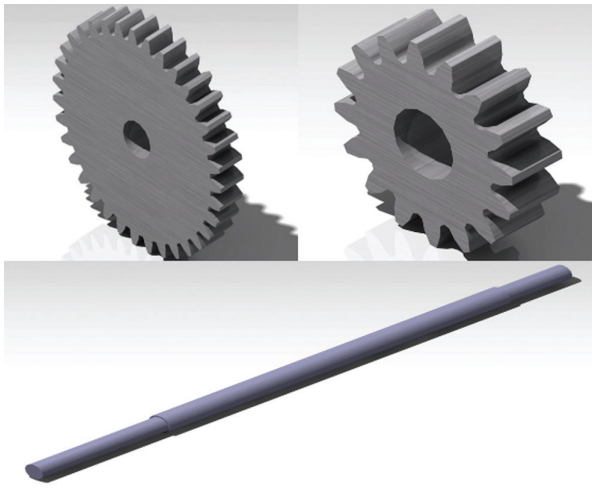

Fig. 4. Depicts the CAD model of gear, pinion, and shaft.

III. VALIDATION

This section discusses the validation of each component to ensure that it behaves analogously to its ideal physical equivalent. The components are validated based on their static and dynamic behavior. The validations are done to ensure the geometry, material characteristics, mass, and stiffness properties are in accordance with the ideal physical models. For the finite element simulations, various modules of ANSYS Workbench have been used.

A. VALIDATION OF THE SHAFT

The static validation of the shaft is done by comparing the deflection of the shaft from FEM by making one end of the shaft cantilevered while applying the load on the other end against the analytical deflection as in Fig. 5 to validate the geometrical and material properties. Table IV summarizes the deviation for 3 loading conditions of the analytical and FEM deflections. The dynamic validation is performed to validate the natural frequency of the shaft, which is validated for the mass and stiffness properties.

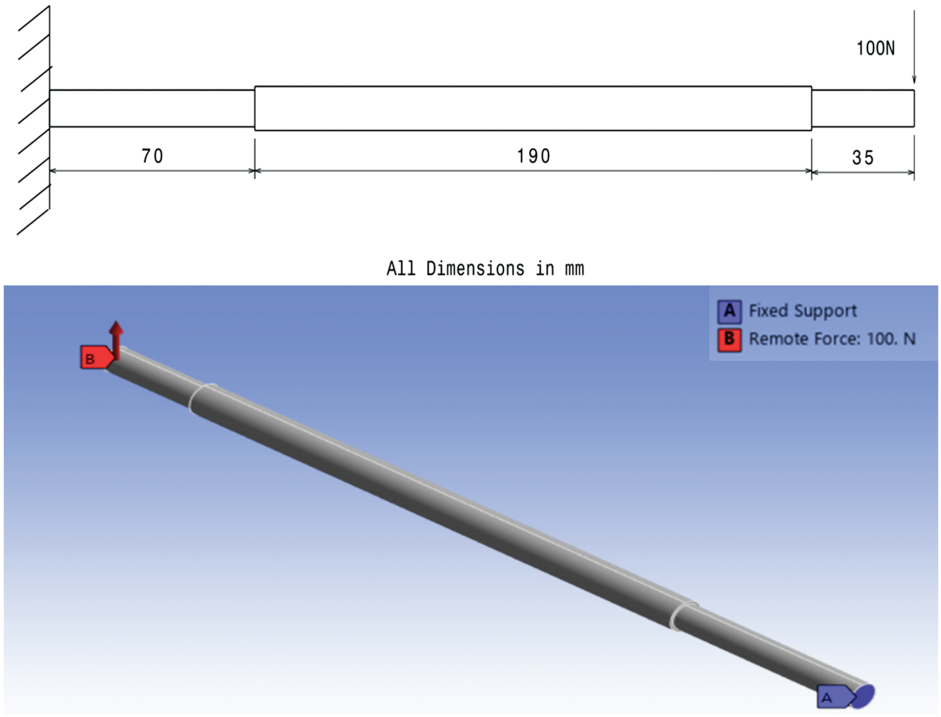

Fig. 5. Depicts the modeling of the shaft for the static validation.

Table IV. Depicts the deflection obtained from ANSYS and analytically

Load applied (N)	Deflection from ANSYS (mm)	Deflection from Castigliano's theorem (mm)	% Deviation
100	6.73	6.72	0.16%
200	13.46	13.43	0.22%
300	20.20	20.16	0.15%

Modal analysis is used for the dynamic validation of the shaft. The analysis is performed for two end conditions: (i) fix-fix ends of the shaft and (ii) free-free ends of the shaft, ensuring the behavior of the shaft remains validated against all other intermediate conditions. Figure 6(a) and 6(b) depict the analytical FE model and the simulation setup in ANSYS Workbench, respectively. The validation data is mentioned in Table V, indicating the first 3 fundamental frequencies within 4% deviation.

B. VALIDATION OF GEAR PAIR

The validation of the gear pair is done in 2 parts: first, the kinematic validation of the gear pair ensures proper meshing and correct modeling of the ideal involute gear tooth profile and then is followed by validating the meshing stiffness, which essentially takes care of the flexibility and contact. For simulation, the pinion is given a constant rotational velocity of 100 rad/s for a period of 0.063 s with a surface mesh size of 0.5 mm elements and the gear ratio is calculated. The setup is depicted in Fig. 7, where the gear and pinion are under mesh. The instantaneous gear ratio lies within 6% of the ideal gear ratio, which is mainly attributed to the contact ratio effect. The average gear ratio comes out to be 2.1870 against the ideal gear ratio of 2.1875, which accounts for 0.02% deviation. Figure 8 depicts the gear mesh mode, where gear teeth are taken as ideal involute profiles.

For the mesh stiffness validation, analytical models are initially formulated, taking the stiffness of the gear tooth, pinion tooth, and contact mesh stiffness into consideration, and then benchmarked with equivalent stiffness obtained from FEM. Figure 9 shows the schematic used for deriving the energy expressions and further development of the gear mesh stiffness formulations. The relevant dimensions of gears are obtained from Table II. X and Y denote the Cartesian coordinate system; X' and Y' denote the transformed coordinate system where the Y' axis is aligned along the axis of the tooth, dy' denotes the elemental section thickness of the tooth at distance y' measured along the Y' axis, β is the involute angle or polar angle of the involute profile, λ is the angle between the start of the involute at the base circle and the line of symmetry passing through the tooth, α_c is the angle made by the force acting normally to the involute profile with the line perpendicular to the line of tooth symmetry, ψ denotes the angle made by the instantaneous normal to the involute with respect to the Y axis. F is the force acting at point C normal to the tooth, and $r_{inv}(\psi)$ is the radial distance from the origin to the instantaneous point on the involute curve. The various dimensions of each gear and pinion have been summarized in Table VI.

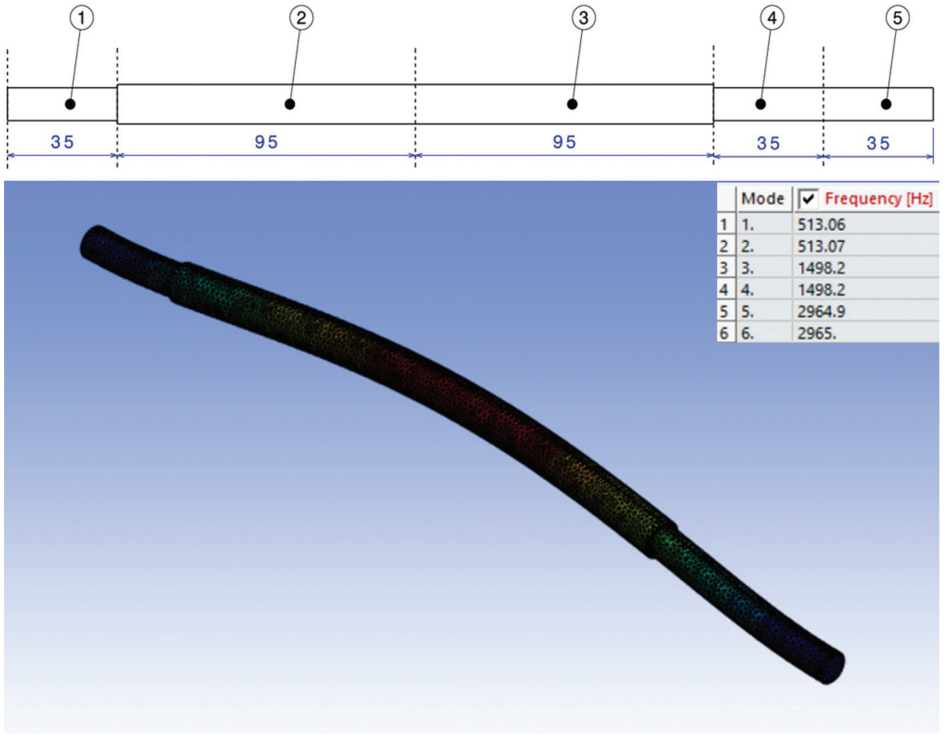

Fig. 6. (a) Depicts the FE model used for analytical modeling, (b) the 1st mode shape and frequencies obtained in both transverse planes.

Table V. Benchmarking ANSYS simulation frequencies against the analytical solution

Sr. No.	Boundary condition	Mode no.	Mode type	Natural frequency (Hz) from theoretical calculations	Natural frequency (Hz) from ANSYS simulation	% Deviation
1	Fixed-fixed	1	Transverse	510.05	513.06	0.59%
		2	Transverse	1484.74	1498.2	0.91%
		3	Transverse	2869.04	2964.9	3.34%
2	Free-free	1	Transverse	664.58	669.67	0.77%
		2	Transverse	1669.73	1685.3	0.93%
		3	Transverse	3018.52	3138.5	3.97%

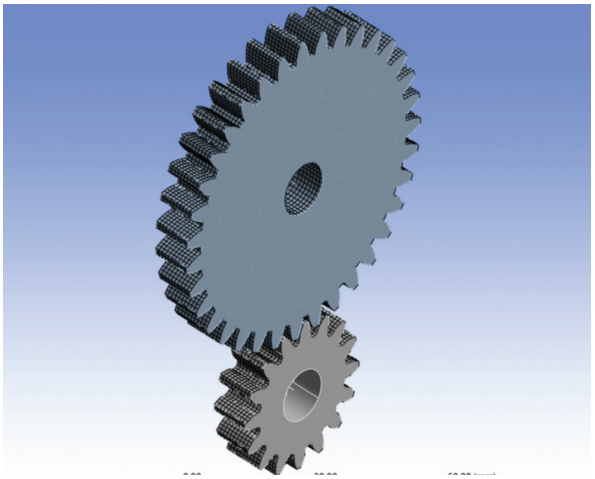

Fig. 7. Setup for rigid dynamic analysis of gear pair in ANSYS workbench.

The parametric equation for the involute profile is given as

$$x = R_b(\sin\psi + \psi\cos\psi)\,, y = R_b(\cos\psi - \psi\sin\psi) \quad (4)$$

The width of the tooth is determined to be $e(\psi) = 2r_{inv}(\psi)\sin(\lambda - \beta)$. The strain energy and stiffness expressions are mentioned as

$$U_t = U_b + U_a + U_s \quad (5)$$

with $U_b = \int \frac{M^2 dy'}{2EI}$; $U_s = \int \frac{S^2 dy'}{2A_r G}$; $U_a = \int \frac{F^2 dy'}{2AE}$; and

$$k_{st} = \frac{F^2}{2U_t} \quad (6)$$

where U_b is the bending energy, U_s shear energy, U_a axial compression energy, E and I denote Young's modulus of the gear material, and P, M, and S denote the load, moment, and shear force, respectively. The integration is carried out using the Gauss quadrature due to the high level of complexity involved with the implicit expressions, and the convergence was observed with 120 Gaussian points. Figure 10 depicts the setup to determine the tooth stiffness

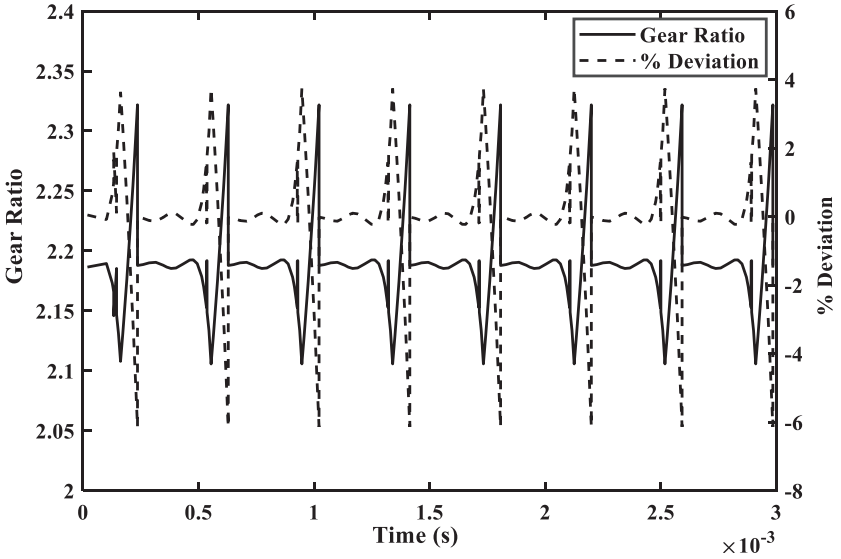

Fig. 8. Variation of gear ratio during gear meshing obtained from the ANSYS simulation.

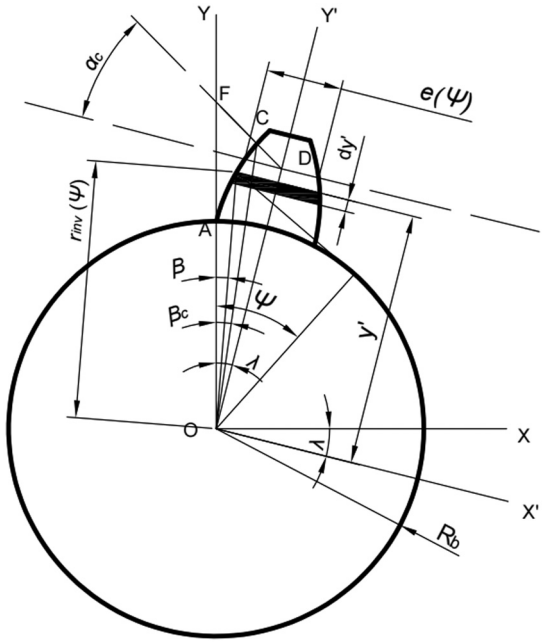

Fig. 9. Model used for determining tooth stiffness.

in ANSYS with a load applied at the tip of the gear. Table VII compares the tooth stiffness for gear and pinion obtained analytically, and that from FEM using the force-deflection curve in Fig. 11, indicating a deviation of 6.41%. This accounts for the portion of the tooth up to the involute profile, and the tooth fillet stiffness is disregarded in the analysis. The analysis also considers the gear body stiffness, which increases the overall stiffness.

Table VI. Various dimensional parameters for gear and pinion

Parameter	Pinion	Gear
β_l	0°	0°
β_u	4.29°	2.26°
λ	6.48°	3.43°
R_b	15.04 mm	32.89 mm

Once the tooth stiffness is validated, the validation for contact mesh stiffness is performed. Marafona *et al.* [22] stated that contact stiffness mainly refers to the stiffness related to the instantaneous point of contact of gears in mesh. Contact stiffness plays a vital role in determining the gear dynamics and, hence the overall characteristic of the gear rotor system and is greatly influenced by any minor deviations in tooth profile. Marafona *et al.* [22] discussed three main approaches to calculate the gear tooth compliance, y_h, which are mentioned in equations (7) through (9).

1) Hertzian and compression approach used as Hamilton Standard [22]:

$$y_h \approx \frac{4F}{\pi b}\left[\left(\frac{1-v_1^2}{E_1}\right)+\left(\frac{1-v_2^2}{E_2}\right)\right]\left[1+\frac{\pi}{4}\right] \tag{7}$$

2) Semi-empirical approach developed by Palmgren [22]:

$$y_h=\frac{4(1-v^2)F}{\pi E_{12} b}\left\{1.10\frac{b^2E_{12}}{F}\right\}^{0.1} \text{ with } E_{12}=\frac{1}{2}\left(\frac{1}{E_1}+\frac{1}{E_2}\right) \tag{8}$$

3) Closed-form approach developed by Weber [22]:

$$y_h = \frac{2F}{\pi b}\left[\left(\frac{1-v_1^2}{E_1}\right)\left\{\ln\left(\frac{2h_1}{b_H}\right)-\left(\frac{v_1}{2(1-v_1)}\right)\right\} + \left(\frac{1-v_2^2}{E_1}\right)\left\{\ln\left(\frac{2h_2}{b_H}\right)-\left(\frac{v_2}{2(1-v_2)}\right)\right\}\right] \tag{9}$$

with, $b_h = \left[\frac{(4F/\pi b)\{(1-v_1^2/E_1)+(1-v_2^2)/E_2\}}{[1/\rho_1+1/\rho_2]}\right]^{\frac{1}{2}}$

where b_h is the half Hertz contact width, subscripts 1 and 2 denote the pinion and gear respectively, h_1 and h_2 are the distances on the pinion and the gear between the point of contact and the tooth centerline along the line of action and ρ_1, ρ_2 are the curvature radii of the pinion and gear

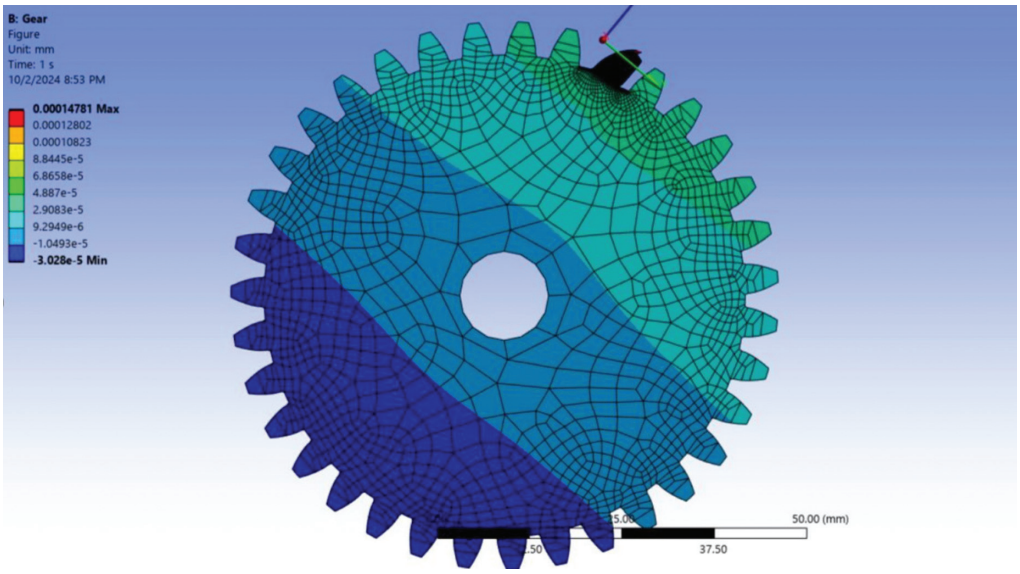

Fig. 10. Setup for tooth stiffness determination in ANSYS static structural workbench.

Table VII. Summary of pinion and gear tooth stiffness obtained analytically and ANSYS simulation

Particular	Pinion stiffness analytically (N/mm)	Stiffness from ANSYS (N/mm)	% Deviation
Pinion	457520.03	428210.52	6.41%
Gear	352612.75	328127.05	6.93%

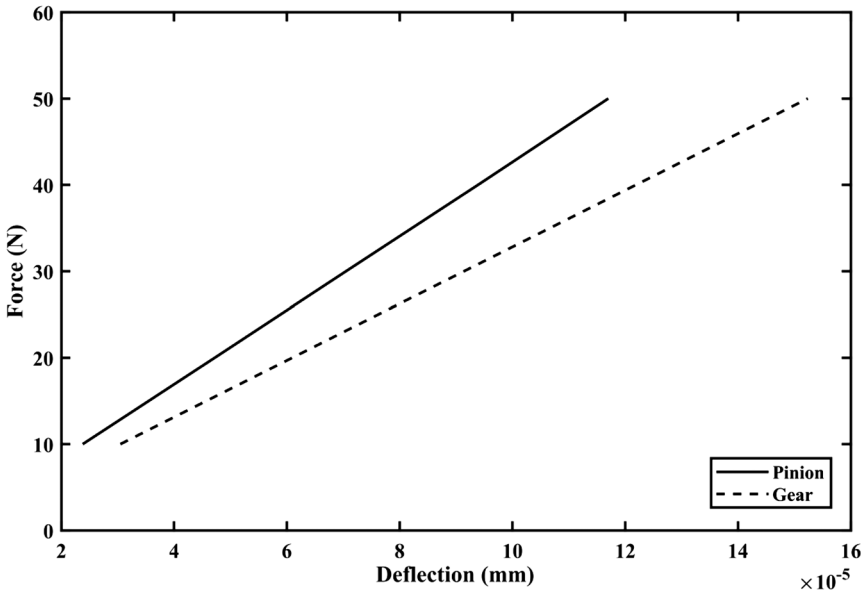

Fig. 11. Force-deflection curve for determining pinion and gear tooth stiffness.

respectively, and E_1, υ_1 and E2, υ_2 denote the Young's modulus and Poisson's ratio of pinion and gear material, respectively, and F is the force. The contact stiffness is then given by: $k_h = \frac{F}{y_h}$. The three models for mesh stiffness are evaluated using equations (7)–(9). The contact stiffness using the Hertzian and compression approach is found to be 9.43×10^5 N/mm, which becomes constant and thus independent of force. The mesh stiffness variation obtained from Palmgren and Weber model is depicted in Fig. 12(a) and 12(b), respectively. For FE modeling, the angle of action for the pinion is divided into 15 incremental steps, with the initial contact point to be taken as 0° and gradually an increment of 0.306° is given to the pinion and the contact stiffness is evaluated. The hub of the gear is fixed, and torque is applied on the pinion, which is free to rotate about its axis. Contact elements are deployed to capture the contact stiffness accurately. Figure 13 summarizes the setup for the FE modeling that is used in the ANSYS

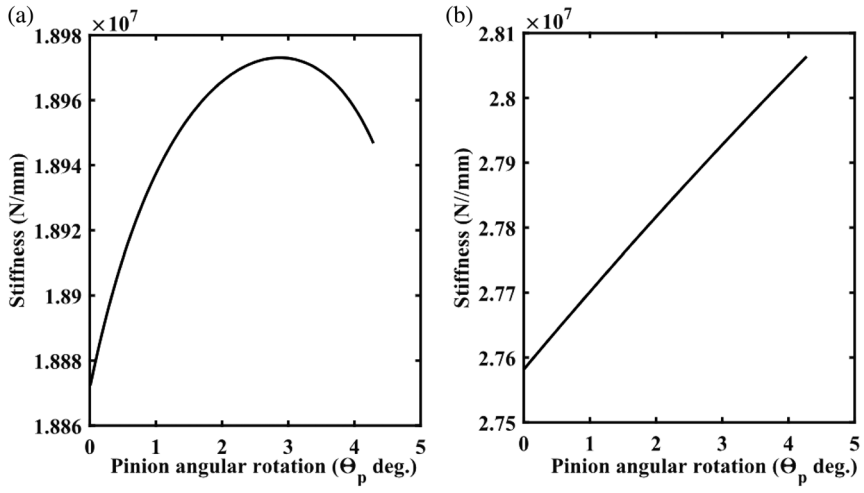

Fig. 12. Contact stiffness-pinion angular rotation as obtained by the (a) Weber model (b) and Palmgren model.

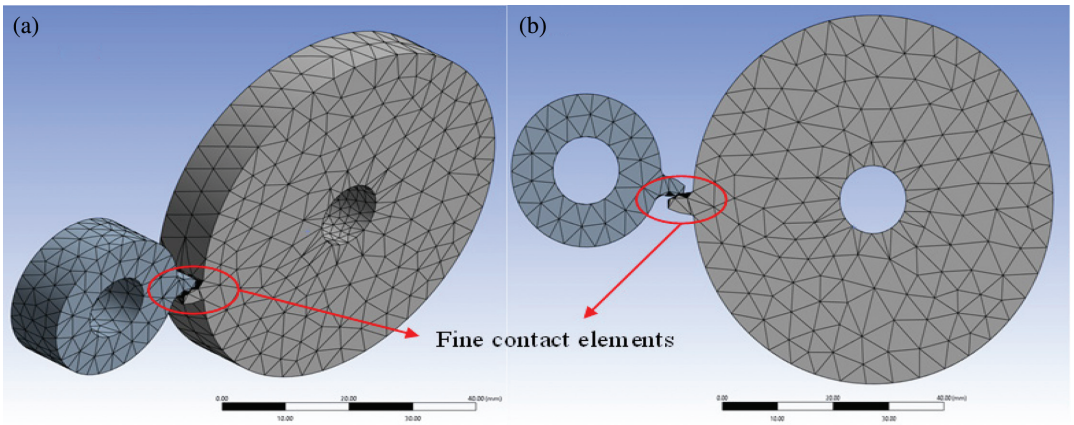

Fig. 13. Depicts the setup for gear mesh stiffness analysis in ANSYS workbench (a) Isometric view (b) and Front view.

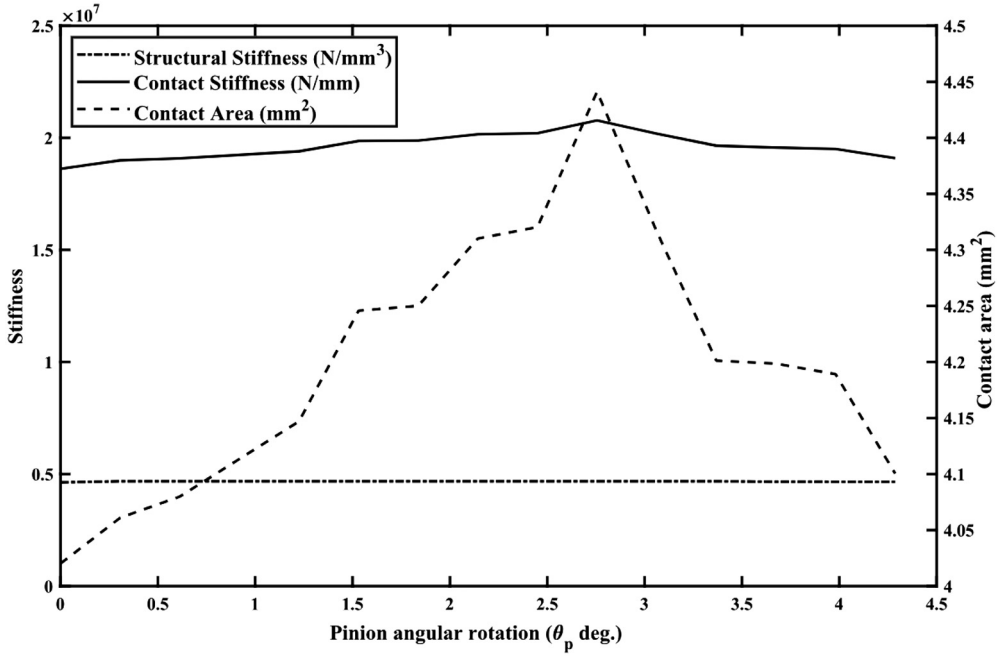

Fig. 14. Variation of contact stiffness with angular rotation of the pinion; the primary axis depicts the stiffness values, and the secondary axis depicts the contact area values.

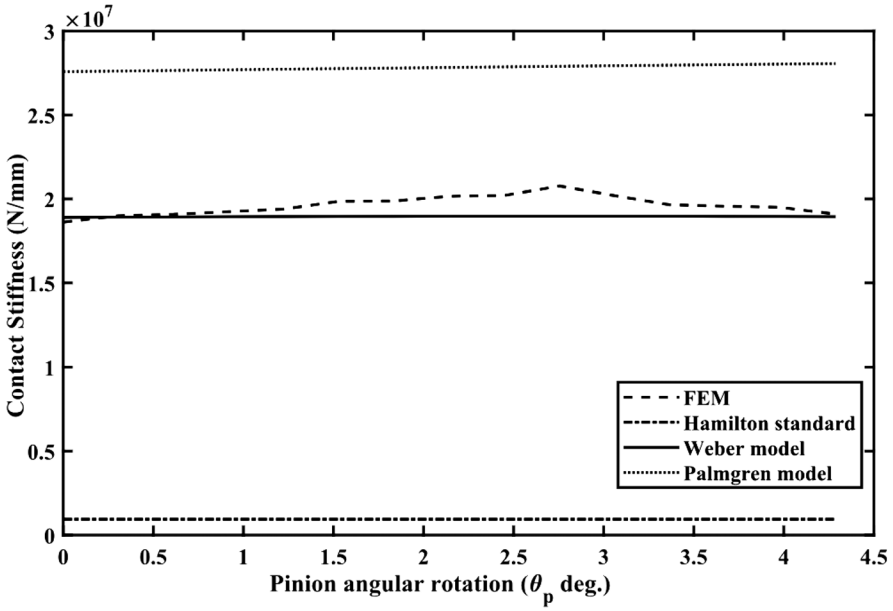

Fig. 15. Comparison of analytical models and finite element models for contact stiffness.

environment. Figure 14 depicts the contact stiffness and contact area as the meshing occurs. The contact stiffness starts from an initial value of 1.863×10^7 N/mm at $\theta = 0°$ and reaches a maximum value of 2.083×10^7 N/mm at an angular rotation value of $\theta = 2.76°$, after which it starts decreasing and reaches a value of 1.913×10^7 N/mm. Figure 15 compares the contact stiffness values from FEM against analytical models, where it agrees closest with the Weber model with a maximum deviation at $\theta = 2.76°$ stands at a 9.48%. It is due to the FE model couples the stiffness of the gear body and leading to deviation from the ideal line contact at all instances during the meshing of the gears. Thus, the overall stiffness of the meshing model is given by $k^{tp} = \frac{1}{1/k_1^{st}+1/k_2^{st}+1/k_h}$, where k_1^{st} is the pinion tooth stiffness and k_2^{st} is the gear tooth stiffness. The maximum stiffness therefore obtained from FEM deviates by maximum 6.66% against the stiffness obtained analytically.

C. SUB-ASSEMBLY AND ASSEMBLY VALIDATIONS

This section discusses the sub-assembly and system assembly validations. The validation performed ensures the correct modeling of contacts and boundary conditions, and accurate meshing of the gear pair. The modal analysis is carried out to validate the dynamic behavior. The pinion and gear are taken to be rigid for sub-systems while flexible for final assembly validation, and the shaft is taken as a flexible body for both cases. For validating the finite element solid element data, the 1-D FE analysis is carried out. The 1-D FE analysis is carried out using 8 beam elements [14], neglecting the material damping of the shaft. The boundary conditions for the free-free case result in the shear force and the bending moment being zero at the free ends, while for fix-fix end conditions result in displacement and slope at the fixed end are set to zero for sub-system validation. Table VIII summarizes the deviations of frequencies obtained from the solid model and the 1-D model using FEM for the sub-assemblies. For system validation, two frequencies are considered: the fundamental transverse and torsional frequencies. The fundamental transverse frequency is obtained experimentally [23], whereas the torsional frequency is obtained using 1-D FEM [14]. The bearings and coupling ends are modeled as remote displacements with bending and rotation allowed. Figure 16 depicts the torsional mode of vibration for the system. Table IX summarizes the deviation of natural frequencies of the digital model against the equivalent physical/1-D FEM analytical model.

The deviations in the 1-D model and solid model FE simulations are attributed to the following reasons: (i) In the torsional case, with the 1-D model the gears are rigid bodies whereas in the 3-D model the gears are taken as flexible bodies to mesh, (ii) Cases with fix-fix boundary condition have more deviation as in 3-D model several nodes are restricted from displacement, unlike the case in the 1-D model, thus adding to some artificial stiffness. Some possible deviations are expected of the physical system

Table VIII. Represents the validation data for sub-systems

Particular	Boundary condition	Natural frequency (Hz) from 1-D FEM	Natural frequency (Hz) ANSYS simulations	% Deviation
Shaft with Pinion	Fix-Fix	424.08	435.27	2.64%
	Free-Free	625.52	634.54	1.44%
Shaft with Gear	Fix-Fix	273.7	279.4	2.08%
	Free-Free	536.49	547.43	2.04%

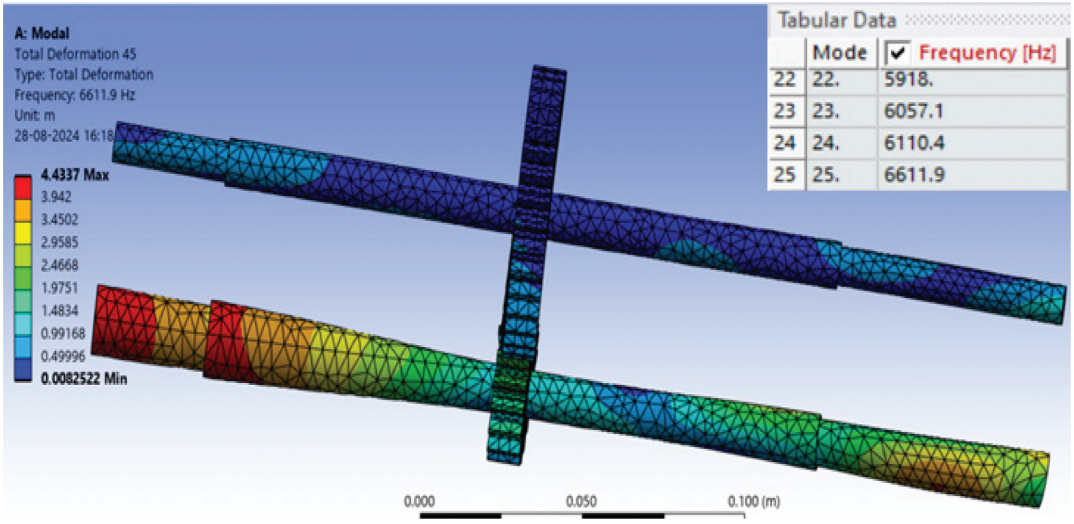

Fig. 16. A snip of modal analysis workbench depicting torsional frequency and mode shape.

Table IX. Benchmarking the fundamental natural frequency of the system obtained from 3-D model against the test rig and 1-D model

Frequency Type	Fundamental natural frequency from test rig/1-D FEM (Hz)	Fundamental natural frequency (Hz) from ANSYS	% Deviation
Transverse	234.00 (Experimentally)	217.45	7.07%
Torsional	6611.9 (Analytically)	6112.23	7.56%

components with the 3-D model, which is mainly attributed to the following reasons: lack of homogeneity and isotropy in the 3-D models, tolerances involved in manufacturing, and unbalances in the physical system.

D. BEARING LINEARIZATION

Bearing forms an essential component of the experimental rig setup as the complex dynamics of the bearing has a major effect on the overall dynamics of the system. The inclusion of the bearing CAD model possesses two main challenges: the complex geometry of the bearing elements (such as balls, races, and their eventual contact) making it computationally expensive and the non-linear behavior of the bearing further makes the analysis of the system complicated. Thus, a simplified approach has been used here to include the bearing dynamics in the operating force range of the model by linearizing the bearing and treating it as a spring model. For the slow and moderate speeds, deep-groove ball bearings subjected to a radial load that causes the radial deflection only (axial deflection being zero), the force-deflection equation given by Palmgren [24] is

$$\delta_r = 4.36 \times 10^{-4} \frac{Q_{\max}^{2/3}}{D_b^{1/3} \cos \alpha} \tag{10}$$

where δ_r is the displacement (m) in the radial direction due to the maximum rolling element load $Q_{\max}$ (N), D_b is the diameter of the ball (m) and α is the contact angle (deg.). The value for the parameters is mentioned in Table X. for the bearing are $\alpha = 0°$ and $D_b = 4.764$ mm and $Q_{\max}$ expression is obtained using Stribeck's equation [24] for the radial load, F_r. Considering a resisting torque of 0.5639 N^{-m}, which is being implemented with the help of a magnetic brake on the gear shaft. The forces acting in the tangential and radial directions on bearing are obtained as in Table X. The bearing is then linearized using equation 10 in the obtained force range and the stiffness values are mentioned in Table XI.

Table X. Load acting on bearings

Bearing location	Direction with respect to the line of action	Load (N)
Input shaft	Tangential	7.65
Input shaft	Radial	2.93
Output shaft	Tangential	9.63
Output shaft	Radial	2.93

Table XI. Stiffness value obtained for bearings

Sub-assembly	Parameter	Value (N/m)
Gear-Shaft	k_{gr} (Radial stiffness)	11934.94
	k_{gt} (Tangential stiffness)	17785.13
Pinion-Shaft	k_{pr} (Radial stiffness)	11934.94
	k_{pt} (Tangential stiffness)	16753.82

IV. MODELING OF PROFILE DEVIATION AND SIMULATIONS

To model the profile deviations exactly, the "web plot digitizer" app was used, which involves the coordinate extraction of actual gear profiles from the gear chart provided by the manufacturer. The required profile is grade 6 as per DIN standards. Any grade higher than this is considered

faulty, and lower grades are considered non-faulty. The different profile deviations for each of the 40 fault cases are summarized in Table XII. For brevity, only the first 4 faults are depicted in Fig. 17. The faults are assumed symmetrical on the tooth, and each of the gear teeth has the same profile to shorten the simulation time. Practically varying deviations can be seen as a superposition of various single deviations. The pinion and gear are bonded to the shaft. The coupling between the input shaft and the motor is replaced by a revolute joint at which a constant angular velocity of 14 Hz is applied, which acts as input power supplied to the system by the motor. A resisting moment of 0.5639 N-m is applied to replace the magnetic brake on the gear shaft. The bearings at the shoulders of the shaft are replaced by springs at 4 mm from the shoulders, as in Fig. 18. Further, to ensure proper meshing of gears, a frictionless contact type is used between the gear and pinion teeth. The entire system is meshed with a mesh size of 1.5 mm with an additional contact mesh of 0.5 mm, ensuring proper meshing of gears by validating the gear ratio to be within 0.04% of the ideal gear ratio. The meshing between the gears is formulated using the augmented Lagrange solver method, ensuring efficient formulation of non-linear contact. The data is collected for 40 fault cases as per Table XIII, using four deformation probes in Y and Z directions placed at 30 mm from the gear/pinion on

Table XII. Depicts the F_α for different fault cases

Fault	F_α (μm)	Fault	F_α (μm)	Fault	F_α (μm)	Fault	F_α (μm)
Fault 1	16.5	Fault 11	8.6	Fault 21	4.3	Fault 31	11
Fault 2	10.7	Fault 12	5.8	Fault 22	4.5	Fault 32	`9.2
Fault 3	12.7	Fault 13	5.7	Fault 23	7.8	Fault 33	3.2
Fault 4	22.7	Fault 14	5.9	Fault 24	5.8	Fault 34	4.2
Fault 5	14	Fault 15	6.9	Fault 25	17.5	Fault 35	3.8
Fault 6	11.7	Fault 16	6.4	Fault 26	13	Fault 36	30
Fault 7	11.9	Fault 17	6.1	Fault 27	15.3	Fault 37	4
Fault 8	8.6	Fault 18	6.4	Fault 28	16	Fault 38	5
Fault 9	8.3	Fault 19	3.6	Fault 29	12.4	Fault 39	7.2
Fault 10	8.7	Fault 20	4.3	Fault 30	10	Fault 40	24.9

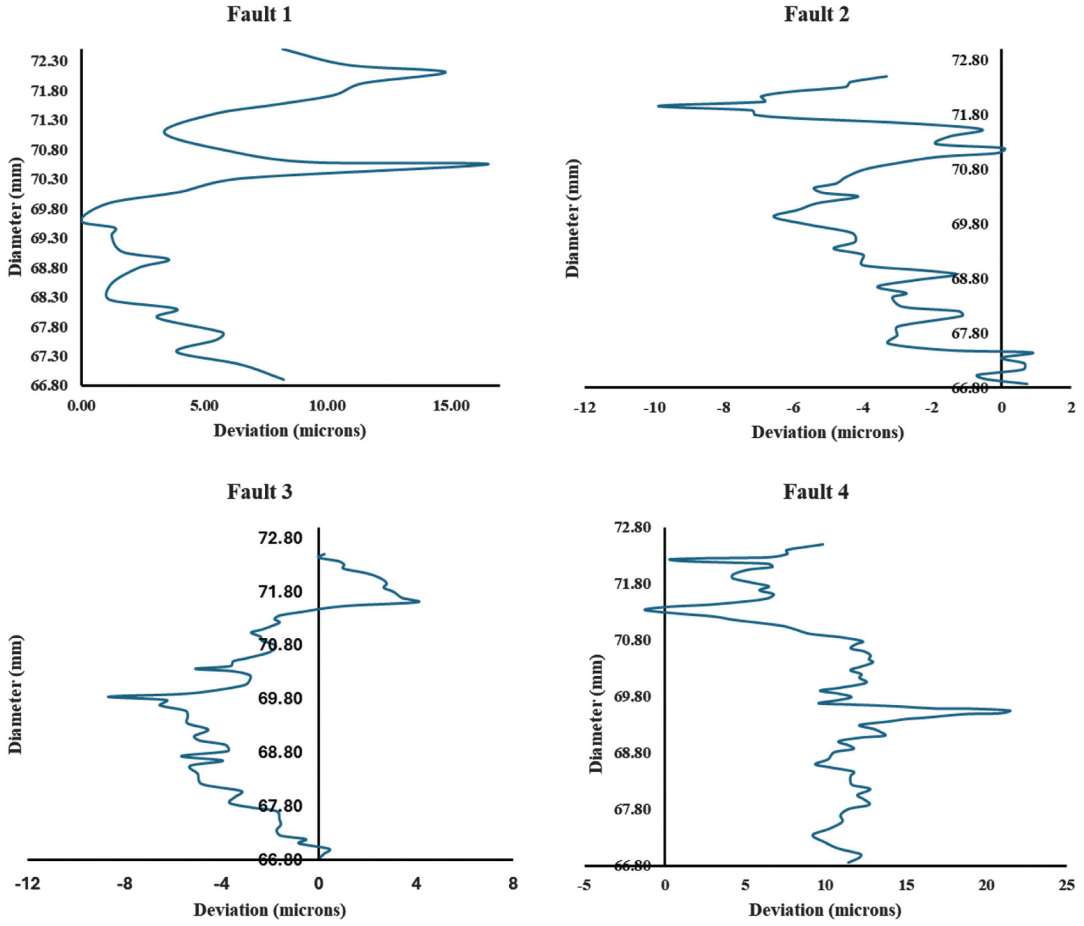

Fig. 17. Profile deviations obtained from gear charts for 1st four fault cases.

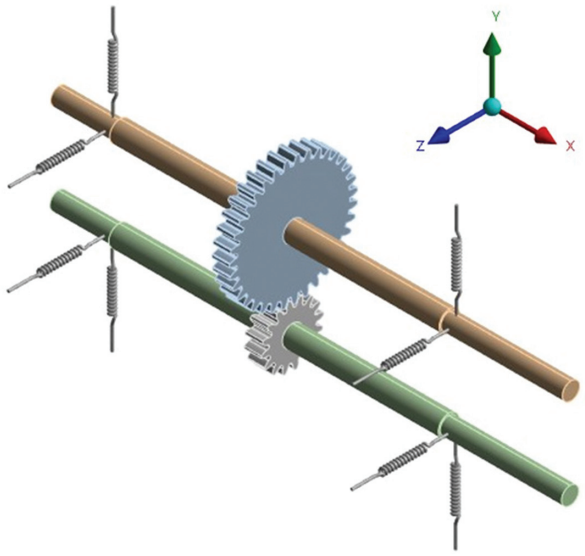

Fig. 18. Model setup in ANSYS Workbench.

Table XIII. Lists the names of the probes and data acquired

Probe	Location
IP1	30 mm from the pinion towards the motor on the input shaft
IP2	30 mm from the pinion towards the free end side of the input shaft
OP1	30 mm from the gear towards the free end side of the output shaft
OP 2	30 mm from the gear towards the magnetic brake on the output shaft

respective shafts at a sampling rate of 1000Hz to accurately capture the meshing frequency. Figure 19 depicts the displacement data for the fault-1 case obtained from the simulation collected using four probes. Further, Table XIV benchmarks the simulation signal against the experimental signal [23] qualitatively, where cross-correlation is used to find the hidden patterns in the experimental signals corresponding to fault cases 11, 10, 9, and 8. An average

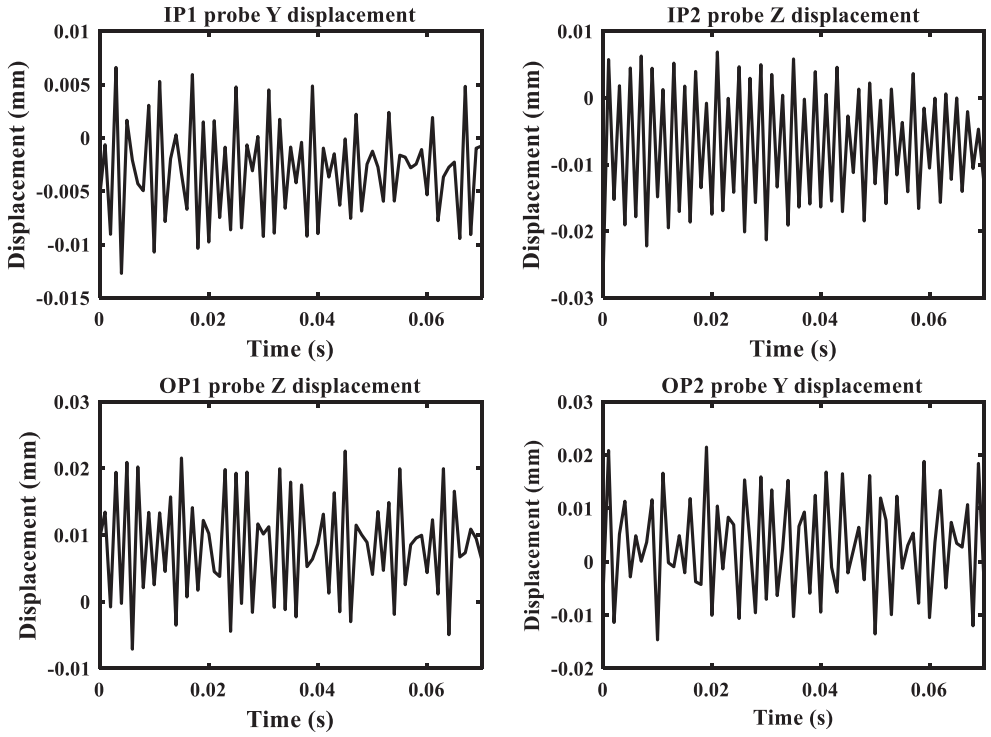

Fig. 19. Depicts the displacement data collected using four probes for fault case 1.

Table XIV. The cross-correlation values of the signals obtained from simulations against the experiment

Fault	Sensor	Correlation value	Fault	Sensor	Correlation value
11	IP1Y	0.49	9	IP1Y	0.49
	IP2Z	0.57		IP2Z	0.59
	OP1Z	0.49		OP1Z	0.51
	OP2Y	0.52		OP2Y	0.51
10	IP1Y	0.49	8	IP1Y	0.51
	IP2Z	0.59		IP2Z	0.60
	OP1Z	0.51		OP1Z	0.50
	OP2Y	0.52		OP2Y	0.48

correlation value of 0.52 is obtained; the deviations are likely due to: replacing the motor and magnetic brake by equivalent boundary conditions, simplified bearing dynamics, unintentional defects in the assembly of the experimental setup, noise in the data acquired through sensors and negligence of profile deviations in the pinion.

V. MACHINE LEARNING

Once the data are acquired, white Gaussian noise is added to make the data more realistic and robust, and then, various statistical parameters for condition monitoring are determined: Energy Ratio (ER), FM0, Crest Factor (CF), Skewness(S), FM4, NA4, RMS, Mean, M6A, M8A, Kurtosis(K), and Standard deviation (SD) [10]. The best signal to predict the fault state is then determined using the Mutual Information (MI). The MI is a measure from information theory that quantifies the amount of information one random variable contains about another, and hence, it is crucial to determine the most informative features with respect to the target variable. The different signals are analyzed, and a particular parameter with the maximum MI score across 8 signals is chosen to be a feature for the development of ML models. Table XV lists the features along with their MI scores and the signal from which they are taken. For dimensionality reduction, further correlations and principal component analysis (PCA) are performed. Table XVI depicts a correlation matrix where M6A is eliminated based on its low MI score and high correlation with M8A. Figure 20 depicts the PCA analysis and the variance of 95% achieved with 8 components.

Table XV. Final list of selected features

Feature	MI Score	Signal
ER	0.2449	OP1Z
FM0	0.2335	IP2Y
CF	0.1690	OP1Y
Skewness	0.1578	OP1Y
FM4	0.1382	IP2Z
NA4	0.1070	IP2Z
RMS	0.0896	OP1Z
Mean	0.0798	IP1Y
M8A	0.0698	IP1Z
Kurtosis	0.0643	IP1Y
SD	0.0643	IP2Z
M6A	0.0546	IP2Y
Total MI Content	1.4729	

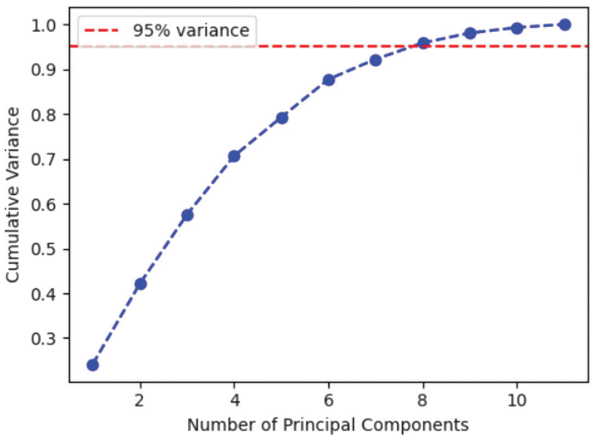

Fig. 20. Variational of the cumulative variance with components in PCA.

Once the PCA components are obtained, the various ML models, namely, Logistic Regression, K-Nearest Neighbor (KNN), Kernel Support Vector Machine (Kernel SVM), Random Forest, and the Artificial Neural Network (ANN) have been implemented and optimized for their best prediction accuracy over the test data, with the aim to carry out binary classification between fault/non-fault case. To ensure better generalization of the models over the data, K-fold validation is used with K=4 folds. Figure 21 represents the performance of various ML models over the selected feature set, where ANN to be best performing with 97.5% prediction accuracy with the optimized parameters and logistic regression to be worst performing with 58.41% prediction accuracy. Table XVII further depicts the optimized hyperparameters identified for different models to get the maximum prediction accuracy, along with the optimized performance.

Table XVI. Correlation matrix for the final set of selected features

Feature/Feature	Mean	SD	S	RMS	K	CF	FM4	M6A	M8A	FM0	ER	NA4
Mean	1.00	–0.03	–0.32	–0.31	0.26	0.12	0.08	0.24	0.03	–0.09	0.11	0.14
SD	–0.03	1.00	–0.14	0.51	0.03	0.21	–0.40	–0.05	–0.22	0.55	0.02	0.60
S	–0.32	–0.14	1.00	0.19	0.18	–0.01	0.22	0.18	0.07	–0.03	0.07	–0.03
RMS	–0.31	0.51	0.19	1.00	–0.02	–0.31	–0.20	–0.01	–0.08	0.36	–0.13	0.01
K	0.26	0.03	0.18	–0.02	1.00	0.37	0.06	0.96	–0.03	–0.31	–0.14	0.04
CF	0.12	0.21	–0.01	–0.31	0.37	1.00	–0.08	0.31	–0.05	–0.17	–0.25	0.45
FM4	0.08	–0.40	0.22	–0.20	0.06	–0.08	1.00	0.12	0.88	–0.17	0.21	–0.15
M6A	0.24	–0.05	0.18	–0.01	0.96	0.31	0.12	1.00	–0.02	–0.27	–0.15	–0.01
M8A	0.03	–0.22	0.07	–0.08	–0.03	–0.05	0.88	–0.02	1.00	–0.11	0.15	–0.04
FM0	–0.09	0.55	–0.03	0.36	–0.31	–0.17	–0.17	–0.27	–0.11	1.00	0.20	0.31
ER	0.11	0.02	0.07	–0.13	–0.14	–0.25	0.21	–0.15	0.15	0.20	1.00	0.16
NA4	0.14	0.60	–0.03	0.01	0.04	0.45	–0.15	–0.01	–0.04	0.31	0.16	1.00

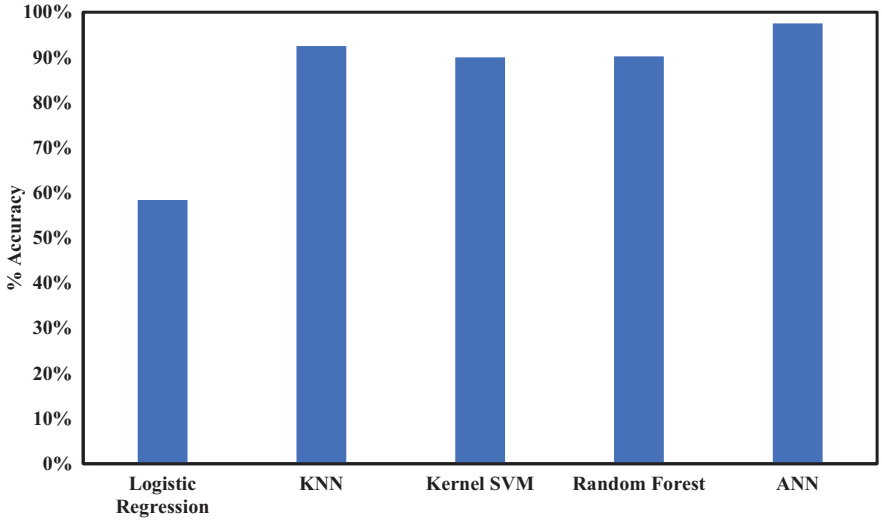

Fig. 21. Illustrates the performance of various ML models over the test set.

Table XVII. Optimized parameters for various ML models

Model	% Accuracy	Optimized parameters
Logistic Regression	58.41%	None
KNN	92.49%	K = 6, where K is the tuning parameter with K nearest neighbors to be considered when classifying
Kernel SVM	90%	Kernel selection with the best performance for the RBF Kernel
Random Forest	90.23%	Number of decision trees: *n*_estimators = 10
ANN	97.50%	Optimizer: Adam, 2 hidden layers with 15 neurons each, Output layer activation function: Sigmoid, Batch size: 5, Epochs: 50

VI. CONCLUSIONS

This work mainly involves studying the effect of profile deviations on gear tooth flanks and predicting them from the dynamic response of the system. The digital model of the system is developed by validating against the equivalent analytical component at each step. The system is dynamically validated against the experimental setup. The different profile deviations are then modeled in the gear in the CAD environment to exactly replicate the deviation present in the tooth of the experimental gears. The response of the system is then collected for different cases in the time domain, and different ML models are then used for binary classification of the system as a fault/no non-fault state using the twelve features extracted from the signal data. The hyperparameters for the ML models are tuned to achieve the maximum prediction accuracy, along with *K*-fold validation to ensure better generalization and a check on overfitting with a limited set of data. The logistic regression model performs poorly, whereas models such as KNN, Kernel SVM with rbf-kernel, and Random Forest are found to be performing with above 90% accuracy, indicating a strong non-linear relationship between the response and the defects, which is likely due to a change in contact non-linearity with the profile deviations. The best performance for the prediction accuracy is obtained using the ANN at 97.5%, which can capture the complex non-linear relationships by optimizing the weights to minimize losses. This concludes that the response of a gear rotor system is strongly dependent on the profile deviation. The future scope involves converting the digital model to a digital shadow, where real-time data integration can be done with the physical model to improve the digital model, ensuring the model is more realistic and robust for performance against the experimental rig setup, which may then be further extended to the concept of digital twin. However, the challenges include high computational resources, the requirement of large data samples and profile deviation modeling, the inclusion of fine dynamics, and complex infrastructure setup for real-time data transfer.

CONFLICT OF INTEREST STATEMENT

The authors declare no conflicts of interest.

REFERENCES

[1] S. S. Ghosh and G. Chakraborty, "On optimal tooth profile modification for reduction of vibration and noise in spur gear pairs," *Mech. Mach. Theory*, vol. 105, pp. 145–163, 2016.

[2] O. D. Mohammed and M. Rantatalo, "Gear fault models and dynamics-based modelling for gear fault detection – a review," *Eng. Fail. Anal.*, vol. 117, p. 104798, 2020.

[3] ISO-1328-1:1997. Cylindrical gears-ISO system of accuracy, 1997.

[4] Y. A. Tesfahunegn, F. Rosa, and C. Gorla, "The effects of the shape of tooth profile modifications on the transmission error, bending, and contact stress of spur gears," *Proc. Inst. Mech.*

Eng. Part C J. Mech. Eng. Sci., vol. 224, no. 8, pp. 1749–1758, 2010.

[5] H. Ma, X. Pang, R. Feng, and B. Wen, "Evaluation of optimum profile modification curves of profile shifted spur gears based on vibration responses," *Mech. Syst. Signal Process.*, vol. 70–71, pp. 1131–1149, 2016.

[6] G. Bonori and F. Pellicano, "Non-smooth dynamics of spur gears with manufacturing errors," *J. Sound Vib.*, vol. 306, no. 1–2, pp. 271–283, 2007.

[7] E. Mucchi, G. Dalpiaz, and A. Rivola, "Elastodynamic analysis of a gear pump. Part II: meshing phenomena and simulation results," *Mech. Syst. Signal Process.*, vol. 24, no. 7, pp. 2180–2197, 2010.

[8] A. Fernández, M. Iglesias, A. De-Juan, P. García, R. Sancibrián, and F. Viadero, "Gear transmission dynamic: effects of tooth profile deviations and support flexibility," *Appl. Acoust.*, vol. 77, pp. 138–149, 2014.

[9] L. F. Zheng, Z. G. Chen, and W. M. Zhai, "Mesh excitations of spur gear considering strong correlation among tooth contact parameters, contact force, and tooth profile deviations," *Sci. China Tech. Sci.*, vol. 66, no. 9, pp. 2500–2516, 2023.

[10] V. Sharma and A. Parey, "A review of gear fault diagnosis using various condition indicators," *Procedia Eng.*, vol. 144, pp. 253–263, 2016.

[11] Z. Chen, Z. Zhou, W. Zhai, and K. Wang, "Improved analytical calculation model of spur gear mesh excitations with tooth profile deviations," *Mech. Mach. Theory*, vol. 149, p. 103838, 2020.

[12] Z. Chen and P. Ji, "Research on the variation of mesh stiffness and transmission error for spur gear with tooth profile modification and wear fault," *Eng. Fail. Anal.*, vol. 122, p. 105184, 2021.

[13] A. Saxena, A. Parey, and M. Chouksey, "Study of modal characteristics of a geared rotor system," *Procedia Technol.*, vol. 23, pp. 225–231, 2016.

[14] R. Tiwari. *Rotor Systems: Analysis and Identification*. Boca Raton, USA: CRC Press, 2018.

[15] L. B. Visnadi, L. N. Garpelli, J. J. Eckert, F. G. Dedini, and H. F. de Castro, "Effect of spur gear crack on rotor dynamic response," *J. Braz. Soc. Mech. Sci. Eng.*, vol. 46, no. 6, p. 331, 2024.

[16] H. Liu, M. Xia, D. Williams, J. Sun, and H. Yan, "Digital twin-driven machine condition monitoring: a literature review," *J. Sens.*, vol. 2022, pp. 1–13, 2022.

[17] W. Kritzinger, M. Karner, G. Traar, J. Henjes, and W. Sihn, "Digital twin in manufacturing: a categorical literature review and classification," *IFAC-Pap. Online*, vol. 51, no. 11, pp. 1016–1022, 2018.

[18] T. Praveenkumar, M. Saimurugan, P. Krishnakumar, and K. I. Ramachandran, "Fault diagnosis of automobile gearbox based on machine learning techniques," *Procedia Eng.*, vol. 97, pp. 2092–2098, 2014.

[19] O. Gecgel, S. Ekwaro-Osire, J. P. Dias, A. Serwadda, F. M. Alemayehu, and A. Nispel. Gearbox Fault Diagnostics Using Deep Learning with Simulated Data. *IEEE International Conference on Prognostics and Health Management*, pp. 1–8, 2019.

[20] I. Lupea and M. Lupea, "Machine learning techniques for multi-fault analysis and detection on a rotating test rig using vibration signal," *Symmetry*, vol. 15, no. 1, p. 86, 2023.

[21] O. Das, D. Bagci Das, and D. Birant, "Machine learning for fault analysis in rotating machinery: a comprehensive review," *Heliyon*, vol. 9, no. 6, p. e17584, 2023.

[22] J. D. M. Marafona, P. M. T. Marques, R. C. Martins, and J. H. O. Seabra, "Mesh stiffness models for cylindrical gears: A detailed review," *Mech. Mach. Theory*, vol. 166, p. 104472, 2021.

[23] P. S. Deshpande and R. Tiwari.*NCCM2024 A Novel Framework for Gear Profile Deviation Detection: Combining Experimental Data with Machine Learning Models.* Presented in 7th National Conference on Rotor Dynamics (NSRD-2024) during 18–20 Dec. 2024, held at SRM Chennai, India.

[24] T. Harris and M. Kotzalas. *Essential Concepts of Bearing Technology*. Boca Raton, USA: CRC Press, 2018.